A Generalized Harmonic Compensation Control Strategy for Mitigating Subsynchronous Oscillation in Synchronverter Based Wind Farm Connected to Series Compensated Transmission Line

Gaoxiang Li, *Member*, *IEEE*, Fujun Ma, *Senior Member*, *IEEE*, Chuanping Wu, Mingshen Li, *Student Member*, *IEEE*, Josep M. Guerrero, *Fellow*, *IEEE* and Man-Chung Wong, *Senior Member*, *IEEE*

***Abstract*—With the increasing application of synchronverter technology in renewable energy power generation, power system stability issue becomes more complicated. Due to the impedance interaction between the synchronverter based wind farm and the series compensated transmission line, the synchronverter based wind farm is prone to cause sub-synchronous oscillation (SSO). To suppress this SSO, a generalized harmonic compensation control strategy of active power filter (APF) with supercapacitor is proposed, which counteracts SSO by injecting the generalized harmonic current including reactive and oscillation current. Since the generalized harmonic current can be calculated by subtracting the sinusoidal active current from the sampling current, a first-order inertial controller of the voltage loop for APF is proposed to accurately obtain the active current. In addition, the supercapacitor of APF is used to reduce the dc-side voltage fluctuation caused by SSO. As this paper does not need to directly extract the SSO component, the proposed method does not need to know the system oscillation frequency in advance, which can be used as a defensive control method of SSO. Finally, experimental results verify the effectiveness of the proposed strategy.**

***Index Terms*—Wind farm, subsynchronous oscillation, supercapacitor, synchronverter, impedance method.**

I. Introduction

BY imitating the mechanism and external characteristics of the synchronous machine (SM), the virtual synchronous machine (VSM) technology is proposed [1]. Due to the characteristics of voltage regulation, frequency modulation and inertia control, the research and application of VSM technology are more and more widespread [2]-[4]. With the increasing application of VSM technology in renewable energy power generation, power system stability issue becomes more complicated [5][6].

Presently, VSM can be categorized into different types based on the different control strategies [7]. So far, the synchronverter specifically refers to the inverter controlled by the VSM control strategy without any closed-loop current or voltage control. Since the impedance of synchronverter is basically inductive, synchronverter can operate stably under weak grid [8]. However, due to the series compensation capacitor, the series-compensated system of synchronverter is prone to cause subsynchronous oscillation (SSO) [9]. In addition, with the increasing application of synchronverter technology in wind farm, the synchronverter based wind farm connected to series compensated transmission line will really exist because the series compensated transmission line is more common in power grid. Thus, it is necessary to study the mechanism, characteristic and defensive method of this SSO.

On the issue of SSO analysis, the widely used ways include frequency scanning method [10], eigenvalue analysis [11], impedance model method [12] and simulation method [13]. Because the impedance model method has the advantages of direct measurement, clear physical meaning and simple form, it has become an important way to analyze system stability [14]. In [15], an impedance network model is proposed to reveal the mechanism and characteristic of the SSO in wind farm. The proposed impedance network model method is similar to the frequency scanning method since they both judge the SSO characteristic by analyzing the resistance and reactance frequency curves of system [16]-[18]. Considering the successful applications of the impedance model method on SSO analysis [19], the impedance model method can be utilized to reveal the mechanism and characteristic of the SSO in wind farm connected to series compensated transmission line.

Moreover, on the issue of SSO mitigation, the common strategies can be divided into two categories: one is to add the additional equipment [20], and the other is to improve the control system [21]-[23]. In some cases, it is necessary to design the additional equipment to suppress SSO because the optimization of control parameter has a limited ability to improve the system stability. In [24], a static synchronous com-

Manuscript received December 19, 2021; revised March 23, 2022 and May 31, 2022; accepted July 9, 2022. This work was supported in part by the National Natural Science Foundation of China (No. 51907010), in part by National Key Research and Development Program of China (No. 2019YFE0118000). Paper no. TPWRS-01939-2021. (*Corresponding author: Fujun Ma.*)

G. Li is with the Guangxi Key Laboratory of Intelligent Control and Maintenance of Power Equipment, School of Electrical Engineering, Guangxi University, Nanning 530004, China (e-mail: ligaoxiang5@163.com).

F. Ma is with the College of Electrical and Information Engineering, Hunan University, Changsha 410082, China (e-mail: mafujun2004@163.com).

C. Wu is with State Key Laboratory of Disaster Prevention and Reduction for Power Grid Transmission and Distribution Equipment, Hunan Province Power Company Disaster Prevention and Reduction Center, Changsha 410100, China (e-mail: jandom@126.com).

M. Li and J. M. Guerrero are with the Department of Energy Technology, Aalborg University, Aalborg 9220, Denmark (e-mail: msh@et.aau.dk; joz@et.aau.dk).

Man-Chung Wong is with the Department of Electrical and Computer Engineering, Faculty of Science and Technology, State Key Laboratory of Internet of Things for Smart City, University of Macau, Taipa 999078, China (e-mail: mcwong@umac.mo).

pensator (STATCOM) with a voltage controller is proposed to damp SSO by stably controlling ac voltage. The modulation index and phase angle of the designed voltage controller are controlled separately, but the corresponding controller is complicated. In [25], an enhancing grid stiffness control strategy of static synchronous compensator with battery energy storage system (STATCOM/BESS) is proposed to suppress the SSO of wind farm in a weak grid. However, this method is not suitable for the SSO mitigation of series-compensated grid-connected system. As the SSO problem manifests as the current oscillation, SSO can be counteracted by injecting the compensation current with the same amplitude and opposite phase [26]. Since SSO frequency is relatively low, the band pass filter (BPF) is usually applied to extract the subsynchronous component [27]. However, when system oscillation frequency changes, the performance of the BPF based SSO suppression method will decline significantly due to the bandwidth limitation of BPF. Moreover, the BPF based SSO suppression method cannot be utilized to suppress the SSO without knowing the system oscillation frequency in advance [28]. In [29], a low pass filter (LPF) and high pass filter (HPF) are combined as a BPF to get the SSO component in *dq* domain. Since the cut-off frequency of HPF is set to be 10Hz, the time delays of the proposed method are large and it cannot suppress the oscillation which is lower than 10Hz in *dq* domain. The characteristics of the aforementioned SSO suppression methods can be summarized in Table I.

TABLE I
ANALYSIS OF EXISTING SSO SUPPRESSION METHODS

Ref.	Description	Disadvantage
[24]	SSO is damped by stably controlling ac voltage.	The proposed STATCOM cannot directly control reactive power, and the designed controller is complicated.
[25]	SSO is suppressed by optimizing system impedance.	It can only suppress the SSO under weak grid condition.
[26]-[29]	SSO is mitigated by injecting compensation current.	Due to the bandwidth limitation of BPF, SSO suppression performance will degrade when system oscillation frequency changes. Moreover, it needs to know system oscillation frequency in advance.

To address the above issues, this paper no longer directly detects the SSO current. Generally, by subtracting the sinusoidal active current from the sampling current, the generalized harmonic current including reactive current and oscillation current can be calculated out. Then, by compensating the generalized harmonic current, the SSO problem can also be resolved effectively. As the active current phase is same with that of voltage which can be obtained by phase locked loop (PLL), only the active current amplitude needs to be got. Therefore, this paper focuses on the active current amplitude calculation. Based on the power conservation, the PI controller of the voltage loop for active power filter (APF) can automatically obtain the active current amplitude [30]. However, due to the low-frequency power oscillation induced by SSO, the obtained active current amplitude will seriously fluctuate.

In this paper, a generalized harmonic compensation control strategy of the APF with supercapacitor is proposed for mitigating the SSO in synchronverter based wind farm connected to series-compensated transmission line. The main works and contributions are summarized as follows.

1) SSO mechanism and characteristic of the synchronverter based wind farm connected to series compensated transmission line is analyzed. With the increase of series compensation level (SCL), the series-compensated grid-connected system of wind farm based on synchronverter is prone to cause SSO.

2) A first-order inertial controller of the voltage loop for the APF with supercapacitor is proposed, which can effectively suppress the SSO without knowing the system oscillation frequency in advance.

3) The influence of the SSO on APF's dc-side voltage is analyzed theoretically. When the dc-side capacitance is large enough, the dc-side voltage of the proposed APF fluctuates within the allowable range and then it can efficiently suppress SSO.

The rest of this paper is organized as follows: In Section II, the reason why the studied system causes SSO is analyzed based on impedance method. In Section III, the mechanism of the proposed SSO suppression strategy is introduced. In addition, the design process of the proposed first-order inertial controller is carefully described. Experimental results are provided in Section IV. Conclusions are drawn in Section V.

II. SSO ANALYSIS OF SYNCHRONVERTER BASED WIND FARM CONNECTED TO SERIES COMPENSATED TRANSMISSION LINE

Fig.1 shows the configuration of the synchronverter based wind farm connected to series compensated transmission line.

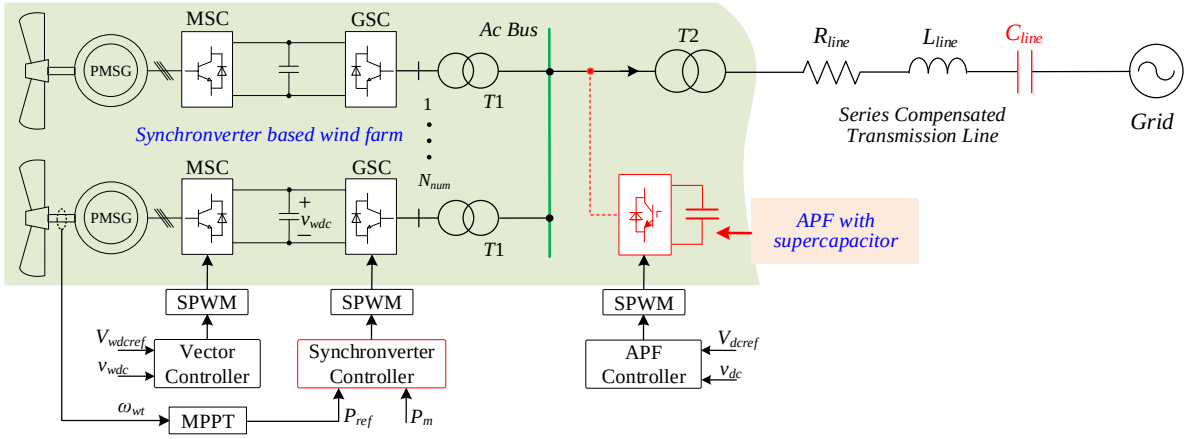

Fig.1. Configuration of the synchronverter based wind farm connected to series compensated transmission line.

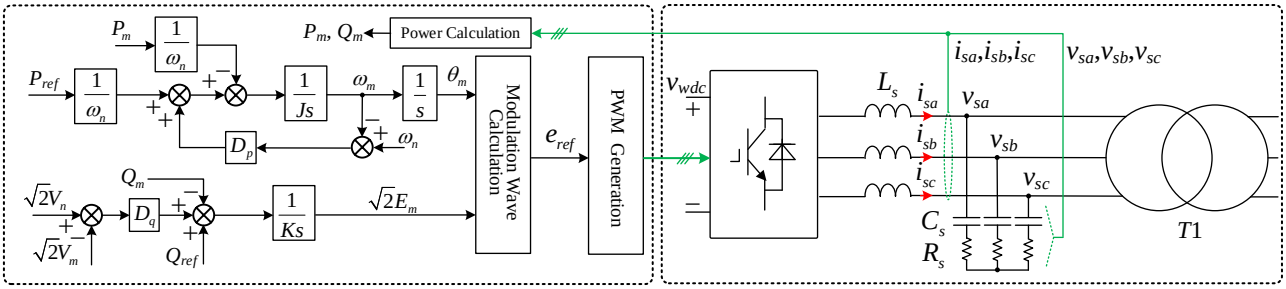

Fig.2. Configuration and control structure of synchronverter.

The generator side converter (GSC) is used to control the dc voltage, and the grid side converter (GSC) is controlled to realize the maximum power point tracking (MPPT). Moreover, the detailed configuration and control structure of the synchronverter are shown in Fig.2, where L_s, R_s and C_s are the inductance, damping resistance and capacitance of the LC filter, respectively; R_{line}, L_{line} and C_{line} are resistance, inductance and capacitance of the series compensated transmission line, respectively; v_{wdc} is the dc-side voltage; i_{sa}, i_{sb} and i_{sc} are the currents of filter inductance L_s; v_{sa}, v_{sb} and v_{sc} are the ac-side voltages.

According to [8], the impedance of synchronverter can be expressed as,

$$Z_s(s)=\frac{0.75V_{ac}M(s-j2\pi f_n)K_d(s)e^{j\theta_d}/\omega_n+sL_s}{1+0.75I_{ac}M(s-j2\pi f_n)K_d(s)e^{j(\theta_d-\theta_{i0})}/\omega_n} \quad (1)$$

where $M(s)=1/(Js^2+D_ps)$; $\theta_d=\arcsin[P_{ref}\omega_nL_s/(E_nV_0)]+\pi/2$; $K_d=1.414E_ne^{-1.5Ts}/[(1+s/\omega_v)(1+s/\omega_v)]$; θ_{i0} is the initial phase of the current. J is virtual moment of inertia; D_p is the active droop coefficient; V_{ac} is ac-side voltage amplitude; I_{ac} is the ac-side current amplitude; ω_n is the rated angular frequency of grid; P_{ref} is the active power reference; E_n is the rated RMS of the modulation wave; f_n is the fundamental frequency; T_s is the switching period; ω_v and ω_i are the cut-off angular frequency of the LPF for voltage and current signals, respectively. The system parameters of Fig.1 and 2 are given in Table II.

TABLE II
SYSTEM PARAMETERS OF FIG.1 AND 2

Parameter	Value	Parameter	Value	Parameter	Value
P_{ref}/kW	10	L_{line}/mH	10	$\omega_v=\omega_i$/(rad/s)	8000π
Q_{ref}/kVar	0	R_{line}/Ω	0.15	ω_n/(rad/s)	100π
V_{wdcref}/V	700	C_{line}/mF	0	f_{pwm}/kHz	10
v_{sa}/V	220	J	0.057	$f_s(1/T_s)$/kHz	10
L_s/mH	3	K	7.1	N_{num}	2
C_s/μF	20	D_q	321	N_{p1}	1/1
R_s/Ω	1.73	D_p	5	N_{p2}	1/1

Fig.3 shows the frequency response characteristics of the synchronverter impedance. In Fig.3, the analytical value of synchronverter impedance is represented by blue solid line. Seen from Fig.3, the synchronverter impedance is mainly inductive and it is good consistent with the measured impedance. Therefore, the stability of the synchronverter based wind farm connected to series compensated transmission line can be analyzed based on the impedance model of synchronverter.

According to reference [4], only the control parameter J is adjustable since other parameters have definite design requirements. Fig.4 shows the impedance frequency characteristics of the synchronverter with different control parameter J. Seen from Fig.4, the control parameter J has little influence on the synchronverter impedance, and synchronverter impedance is mainly inductive. Thus, from the perspective of impedance characteristics, the control parameter optimization of synchronverter has a limited ability to improve the system stability.

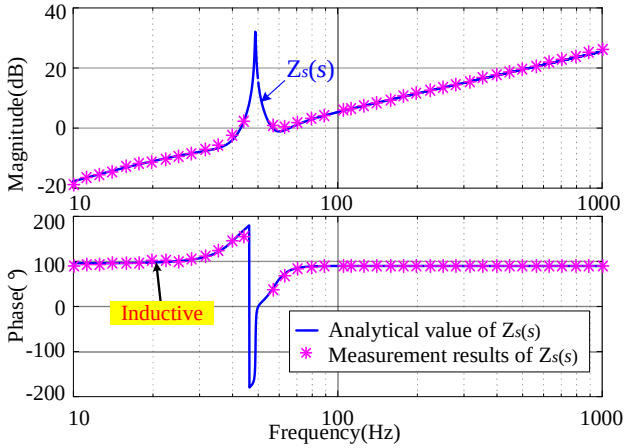

Fig.3. Frequency response characteristics of synchronverter impedance.

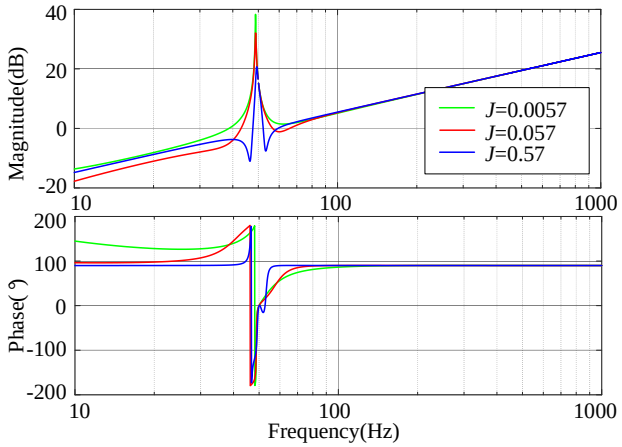

Fig.4. Impedance frequency characteristics of synchronverter with different control parameter J.

For the series compensated transmission line, the *SCL* can be obtained by,

$$SCL=\frac{1}{\omega_n^2L_{line}C_{line}} \quad (2)$$

where ω_n is the rated angular frequency of grid.

This article has been accepted for publication in IEEE Transactions on Power Systems. This is the author's version which has not been fully edited and content may change prior to final publication. Citation information: DOI 10.1109/TPWRS.2022.3191061

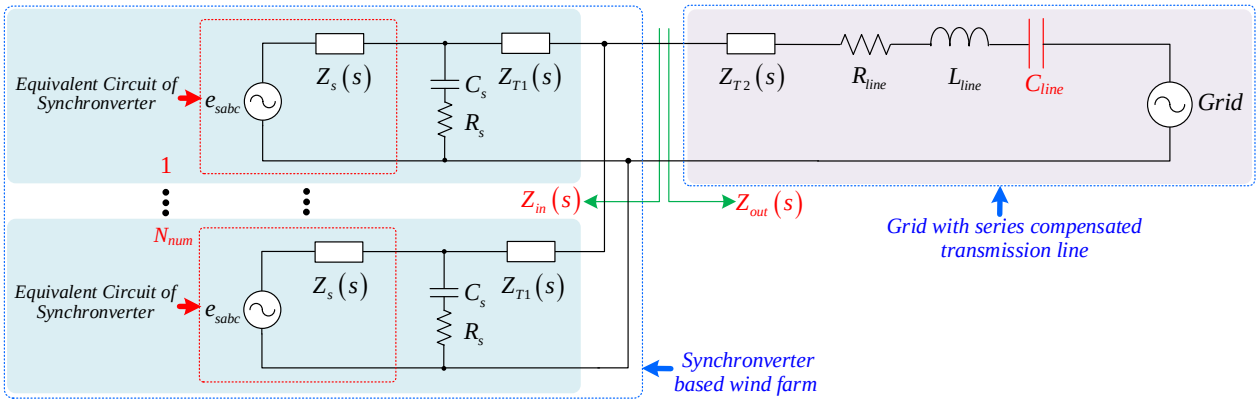

Fig.5. Equivalent circuit of the synchronverter based wind farm connected to series compensated transmission line.

In addition, assuming the synchronverters are the same in the studied wind farm, the equivalent circuit of the studied system can be depicted in Fig.5, where e_{sabc} is the equivalent voltage source of synchronverter; $Z_s(s)$ is the equivalent impedance of synchronverter; $Z_{T1}(s)$ and $Z_{T2}(s)$ are the equivalent impedance of transformer T1 and T2, respectively; $Z_{in}(s)$ is the inner impedance of the synchronverter based wind farm; $Z_{out}(s)$ is the outer impedance of the synchronverter based wind farm; N_{num} is the number of the parallel synchronverters in wind farm; N_{p1} and N_{p2} are the transformer ratio of transformer T1 and T2, respectively. From Fig.5, the impedance $Z_{in}(s)$ can be obtained as follow,

$$Z_{in}(s)=\frac{N_{p1}^2}{N_{num}}\cdot\left[Z_s(s)\,\|\left(R_s+\frac{1}{C_s s}\right)+Z_{T1}(s)\right] \tag{3}$$

In addition, the impedance $Z_{out}(s)$ is obtained as follow,

$$Z_{out}(s)=Z_{T2}(s)+\frac{1}{N_{p2}^2}\left(R_{line}+L_{line}s+\frac{1}{C_{line}s}\right) \tag{4}$$

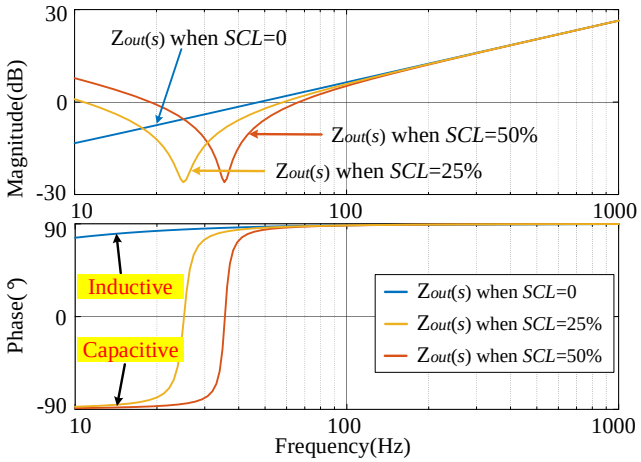

Fig.6. Frequency response characteristics of impedance $Z_{out}(s)$ with different *SCL*.

Fig.6 shows the frequency response characteristics of impedance $Z_{out}(s)$. Seen from Fig.6, after adding the series compensation capacitor C_{line}, partial impedance of $Z_{out}(s)$ changes from inductive to capacitive, and the capacitive impedance range increases with the increase of *SCL*. From Fig.3 and 6, the synchronverter impedance is inductive and the impedance $Z_{out}(s)$ is capacitive in the low-frequency area. Considering that the capacitive impedance easily resonates with the inductive impedance, the series-compensated grid-connected system of wind farm based synchronverter is prone to cause SSO when *SCL* increases.

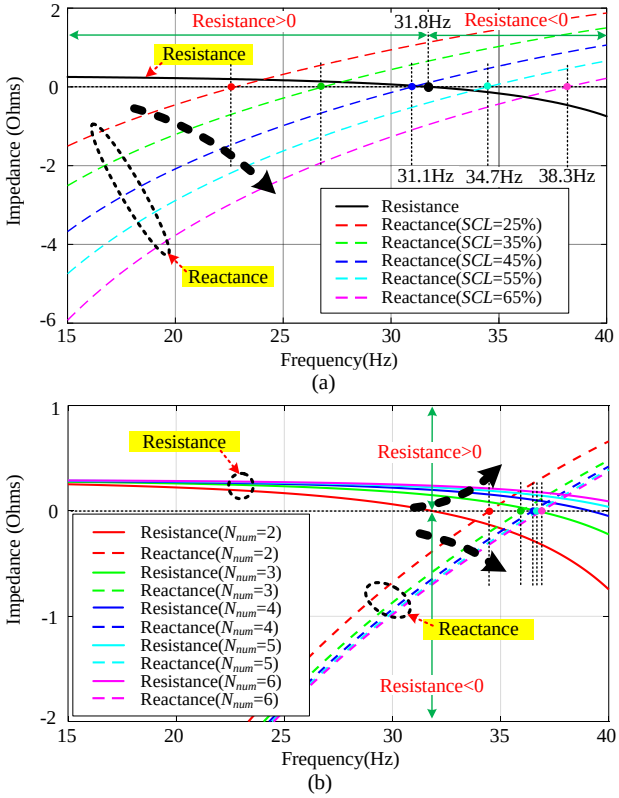

Fig.7. Impedance-frequency curves of the studied system under different conditions. (a) Under different *SCL*. (b) Under different N_{num}.

Fig.7 shows the impedance-frequency curves of the studied system under different conditions. It is well known that the frequency point where the reactance value is zero is the impedance resonance point of system. As seen from Fig.7(a), with the increase of *SCL*, the impedance resonance point of system gradually moves to the high-frequency area. In addition, the system resistance is negative when the frequency is greater than 31.8Hz. According to the impedance network model based SSO analysis method [15], the system is unstable when the resistance of system is negative and the reactance of system crosses the zero-axis with a positive slop (meaning from negative to positive). Therefore, due to the impedance interaction

between the synchronverter based wind farm and the series compensated transmission line, the synchronverter based wind farm will cause SSO with the increase of *SCL*. Moreover, the system oscillation frequency increases with the increase of *SCL*. Seen from Fig.7(b), with the increase of the number of parallel synchronverters, the frequency point where the resistance value is zero moves to the high-frequency area. Meanwhile, the impedance resonance point of system slightly moves to the high-frequency area too. Since the negative resistance of system comes from synchronverter, the negative resistance of system decreases when the number of the parallel synchronverters increases. Thus, when N_{num} increases, the resistance of system becomes large and is positive at the impedance resonance point. Based on the analysis above, with the increase of the number of parallel synchronverters, the stability of the synchronverter based wind farm becomes better and the SSO will not easily occur.

III. A First-Order Inertial Controller of APF with Supercapacitor for Damping SSO

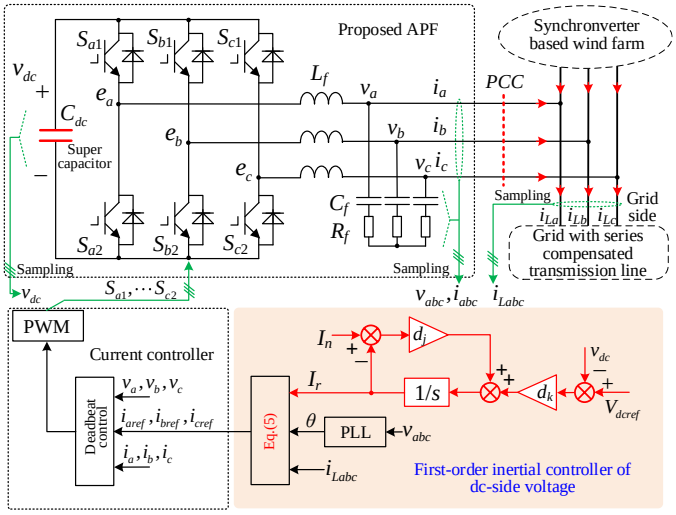

Fig.8. Configuration and control structure of the proposed APF.

TABLE III
SYSTEM PARAMETERS OF FIG.8

Parameter	Value	Parameter	Value	Parameter	Value
P_N/kW	0	L_f/mH	3.2	R_f/Ω	1.17
Q_N/kVar	10	C_{dc}/F	0.1	d_k	10
V_{dcref}/V	750	C_f/μF	20	d_j	100

To suppress this SSO, a APF with supercapacitor is designed and connected in parallel in the studied system, as shown in Fig.1. The proposed APF counteracts the SSO by injecting the generalized harmonic current. Thus, the minimum capacity of the designed APF should be able to compensate the generalized harmonic current. Considering that the SSO current is instantaneous and the power electronics have short-term overcurrent capability, the capacity of the proposed APF can be designed to be half the rated capacity of a given power plant, which is basically consistent with the capacity design of the existing compensators [26][31]. The configuration and control structure of the proposed APF are depicted in Fig.8, where L_f, R_f and C_f are the inductance, damping resistance and capacitance of the LC filter, respectively; v_{dc} is the dc-side voltage; V_{dcref} is the dc-side voltage reference; e_a, e_b and e_c are the inner voltages; v_a, v_b and v_c are the point of common coupling (PCC) voltages; i_a, i_b and i_c are the grid-connected currents; i_{Labc} are the grid-side currents; I_n is the rated active current amplitude of i_{Labc}; I_r is the active current amplitude obtained by the designed first-order inertial controller; θ is the active current phase obtained by PLL; d_k and d_j are the control parameters of the proposed first-order inertial controller. The system parameters of Fig.8 are given in Table III.

In Fig.8, the active currents are calculated out based on the amplitude I_r and phase θ. The references of current loop are expressed as follow,

$$\begin{cases} i_{aref} = i_{La} - I_r \cos\theta \\ i_{bref} = i_{Lb} - I_r \cos(\theta - 2\pi/3) \\ i_{cref} = i_{Lc} - I_r \cos(\theta + 2\pi/3) \end{cases} \tag{5}$$

A. Calculation of active current amplitude

Generally, the ac-side active power P_{ac} of APF is equivalent to the sum of the dc-side active power P_{dc} and active power loss P_{loss}. Therefore, there is,

$$P_{dc} + P_{loss} = P_{ac} \tag{6}$$

In a stable state, the dc-side voltage v_{dc} is approximately equal to V_{dcref} and P_{dc} can be calculated by,

$$P_{dc} = C_{dc}\frac{v_{dc}dv_{dc}}{dt} \approx C_{dc}\frac{V_{dcref}dv_{dc}}{dt} \tag{7}$$

In addition, P_{ac} can be obtained as,

$$P_{ac} = \frac{3}{2}V_0 I_0 \approx \frac{3}{2}V_n I_0 \tag{8}$$

where V_0 is the ac-side voltage amplitude of the proposed APF; V_n is the rated value of V_0; I_0 is the ac-side active current amplitude of APF.

Substituting (7) and (8) into (6), there is,

$$\frac{3}{2}V_n I_0 \approx C_{dc}\frac{V_{dcref}dv_{dc}}{dt} + P_{loss} \tag{9}$$

According to (9), the ac-side active current amplitude I_0 can be obtained as follow,

$$I_0 \approx \frac{2}{3}\frac{C_{dc}V_{dcref}}{V_n}\frac{dv_{dc}}{dt} + \frac{2}{3}\frac{P_{loss}}{V_n} \tag{10}$$

Seen from (10), when the dc-side voltage v_{dc} is stable, the ac-side active current amplitude I_0 will be a very small constant, which is equal to ($2/3*P_{loss}/V_n \approx 0$). Thus, when the proposed APF works normally, there is $I_0 \approx 0$.

In addition, from Fig.8, when voltage v_{dc} is stable, there is,

$$d_j(I_n - I_r) = d_k(V_{dcref} - v_{dc}) \tag{11}$$

The Eq.(11) can be rewritten as,

$$I_r = I_n - \frac{d_k(V_{dcref} - v_{dc})}{d_j} \tag{12}$$

According to (12), I_r is a constant when v_{dc} is stable. From (5), the references of the current loop for the proposed APF are obtained by subtracting the sinusoidal active current from i_{Labc}. Therefore, there is $I_0 \approx 0$ only when the sinusoidal active current amplitude I_r stabilizes at the active current amplitude of i_{Labc}. Based on the analysis above, when the proposed APF

works stably, the output value of the proposed first-order inertial controller will automatically stabilize at the active current amplitude of i_{Labc} due to the power conservation.

B. Design of dc-side capacitor

In this paper, the proposed APF suppresses this SSO by injecting the compensation current with the same amplitude and opposite phase. Considering that SSO is also a cycle oscillation of power, the dc-side capacitor of the proposed APF should be large enough to compensate the periodic oscillation power. In addition, when the dc-side capacitor is large, the fluctuation of the capacitor voltage will be small, which is beneficial to the control of current loop.

When the system causes SSO, the ac-side active power P_{ac} will also appear oscillation. According to energy conservation theory, there is,

$$\frac{P_{sso}T_{op}}{2} = C_{dc}\frac{v_{dc}dv_{dc}}{dt}\frac{T_{op}}{2} \tag{13}$$

where T_{op} is the oscillation period of P_{sso}.

In steady state, the dc-side voltage v_{dc} is approximately equal to V_{dcref}. Therefore, the relationships among the ac-side active oscillation power P_{sso} and dc-side voltage fluctuation $\triangle v_{dc}$ can be obtained as follow,

$$\frac{P_{sso}T_{op}}{2} \approx C_{dc}V_{dcref}\Delta v_{dc} \tag{14}$$

Due to $T_{op}=1/f_{sso}$, (14) can be rewritten as follow,

$$\frac{P_{sso}}{2f_{sso}} \approx C_{dc}V_{dcref}\Delta v_{dc} \tag{15}$$

where f_{sso} is the oscillation frequency.

Fig.9 shows the relationships among the dc-side voltage fluctuation $\triangle v_{dc}$, dc-side capacitance C_{dc}, active oscillation power P_{sso} and oscillation frequency f_{sso}. Seen from Fig.9, with the increase of C_{dc}, the dc-side voltage fluctuation $\triangle v_{dc}$ becomes smaller. In addition, with the decrease of oscillation frequency f_{sso}, the dc-side voltage fluctuation $\triangle v_{dc}$ becomes larger. Moreover, with the increase of active oscillation power P_{sso}, the dc-side voltage fluctuation $\triangle v_{dc}$ becomes larger too. To make the dc-side voltage $\triangle v_{dc}$ fluctuate within an allowable range, the dc-side capacitance C_{dc} should be large enough. Based on the analysis above, supercapacitor is a good choice, which can provide enough energy to damp the SSO and reduce the dc-side voltage fluctuation of APF.

C. Design of first-order inertial controller

From Fig.8, the first-order inertial controller $G_v(s)$ can be obtained as,

$$G_v(s) = \frac{d_k}{s+d_j} \tag{16}$$

According to Fig.8 and Eq.(16), the open-loop transfer function of voltage can be obtained as,

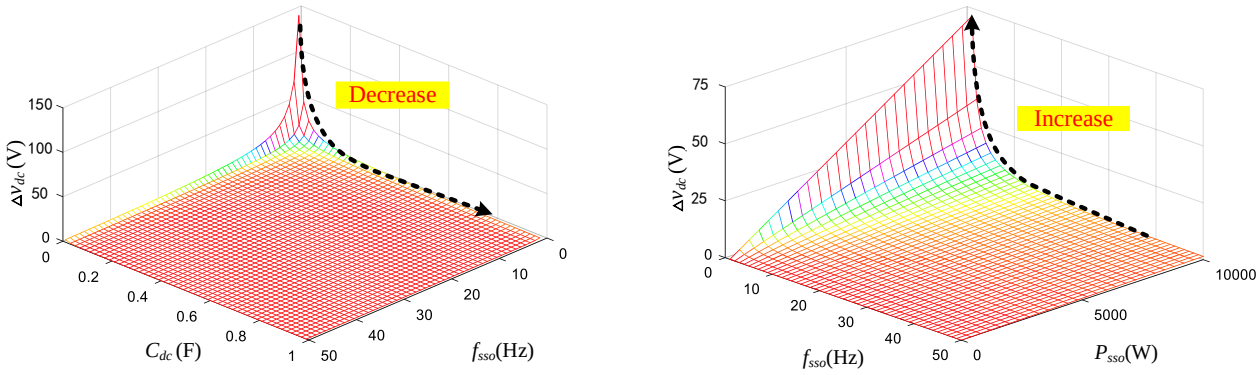

(a) (b)

Fig.9. Relationships among the dc-side voltage fluctuation $\triangle v_{dc}$, the dc-side capacitance C_{dc}, the active oscillation power P_{sso}, and the oscillation frequency f_{sso}. (a) P_{sso}=2000W. (b) C_{dc}=0.1F.

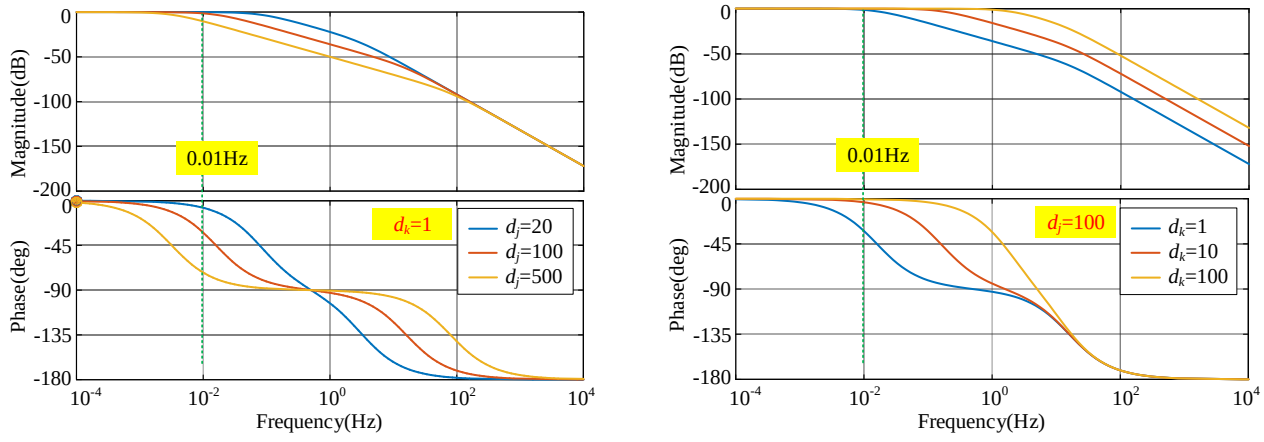

(a) (b)

Fig.10. Bandwidth of the voltage loop with different control parameters. (a) Under different d_j when d_k=1. (b) Under different d_k when d_j=100.

$$G_{v\_op}(s)=G_v(s)G_t(s)\frac{1}{sC_{dc}} \tag{17}$$

where $G_t(s)$ is the inverter delay, expressed as,

$$G_t(s)=\frac{1}{1+1.5sT_s} \tag{18}$$

From Eq.(17), the closed-loop transfer function of voltage can be obtained as,

$$G_{v\_cp}(s)=\frac{G_v(s)G_t(s)}{G_v(s)G_t(s)+sC_{dc}} \tag{19}$$

Fig.10 shows the control bandwidth of voltage loop under different control parameters. Seen from Fig.10(a), with the increase of d_j, the control bandwidth of voltage loop decreases slightly. From Fig.10(b), with the increase of d_k, the control bandwidth of voltage loop increases slightly. From Fig.10, the control parameters have a relatively small influence of the voltage loop and the control bandwidth is very small. Due to the small control bandwidth, the proposed first-order inertial controller can slowly regulate the dc-side voltage to stably obtain the active current amplitude I_r.

In addition, from (12), the dc-side voltage v_{dc} will fluctuate when the active current amplitude I_r changes. To make the dc-side voltage v_{dc} fluctuates within 10% when there is 50% current fluctuation, the control parameters of the designed first-order inertial controller should satisfy the following relationship,

$$\frac{d_k}{d_j}\geq\frac{50\%I_n}{10\%V_{dcref}}=\frac{5I_n}{V_{dcref}} \tag{20}$$

To verify the above theoretical analysis, the studied system, as shown in Fig.1, is built and simulated in MATLAB/Simulink. The system parameters are given in Table II and III, and the simulation step size is designed to be 0.000001s. The simulation results are shown as follows.

Fig.11 shows the comparative simulation results of dc-side voltage v_{dc} and active current amplitude I_r. As seen from Fig.11(a), when *SCL* is increased from 10% to 55%, the dc-side voltage of APF in [30] will markedly fluctuate since the dc-side

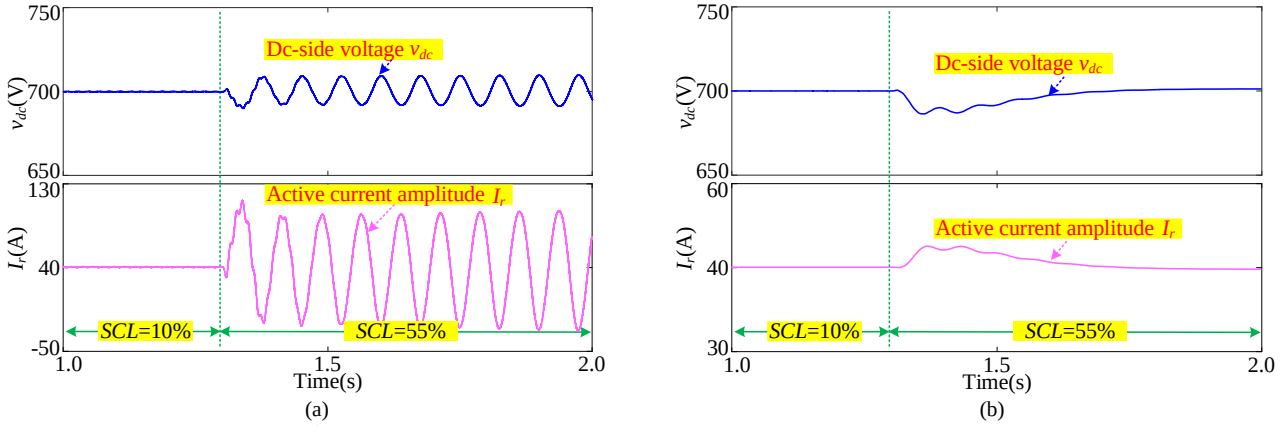

Fig.11. Comparative simulation results of dc-side voltage v_{dc} and active current amplitude I_r. (a) The APF in [30]. (b) The proposed APF.

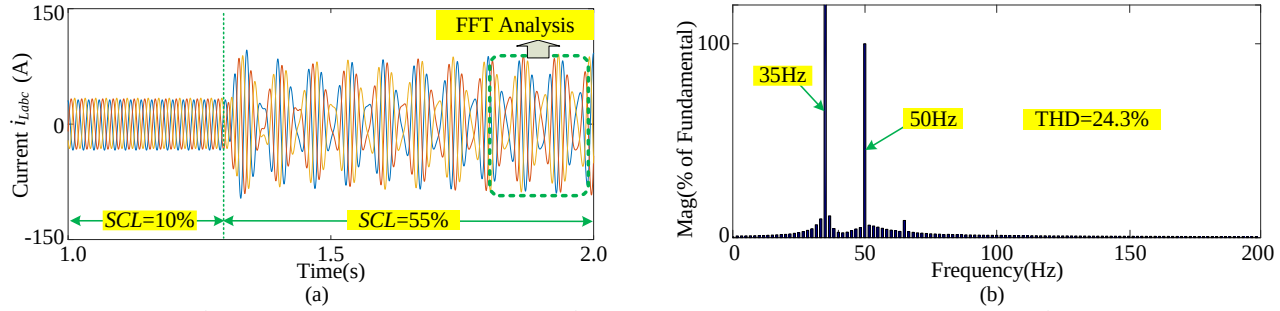

Fig.12. Simulation results of the studied system when *SCL* is switched from 10% to 55%. (a) Grid currents. (b) FFT analysis of current.

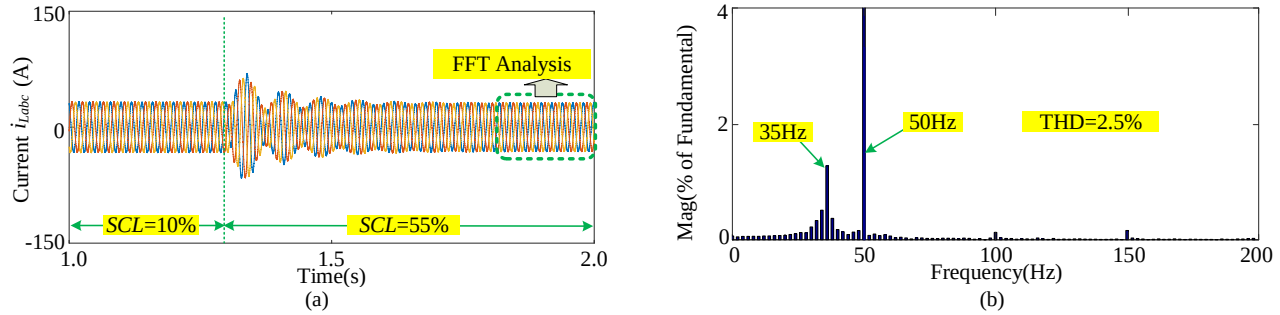

Fig.13. Simulation results of the studied system with the proposed APF when *SCL* is switched from 10% to 55%. (a) Grid currents. (b) FFT analysis of current.

This article has been accepted for publication in IEEE Transactions on Power Systems. This is the author's version which has not been fully edited and content may change prior to final publication. Citation information: DOI 10.1109/TPWRS.2022.3191061

capacitance is small. In addition, as the PI controller of voltage loop cannot filter out this low-frequency oscillation, the obtained active-current amplitude I_r oscillates too. Seen from Fig.11(b), due to the large dc-side capacitance and control inertia of voltage loop, the proposed APF can damp this oscillation and obtain a stable active current amplitude. From Fig.11, the proposed first-order inertial controller of the voltage loop for APF can effectively obtain the active current amplitude I_r, which can provide accurate reference for current inner loop.

Fig.12 and 13 shows the comparative simulation results of the studied system with and without the proposed APF. As seen from Fig.12, without the proposed APF, the series compensation grid-connected system of wind farm based on synchronverter will cause SSO when the *SCL* is increased from 10% to 55%. In addition, the SSO frequency is about 35Hz, which is basically consistent with the results of theoretical analysis. Seen from Fig.13, after adding the proposed APF, the series compensation grid-connected system of wind farm based on synchronverter can finally run stably when the *SCL* is increased from 10% to 55%. In addition, the total harmonic distortion (THD) of grid-connected current is about 2.5%, which meets the THD requirements of power grid. From Fig.12 and 13, the proposed APF can effectively suppress the SSO of the studied system.

IV. Experiments

To further validate the above analysis, the synchronverter based wind farm connected to series compensated transmission line is built based on the RT-LAB platform and DSP+FPGA control board, as shown in Fig.14. The control algorithm is implemented in DSP+FPGA and the circuit is emulated by RT-LAB OP5700. The experimental parameters are listed in Table II and III, and the experimental results are given as follows.

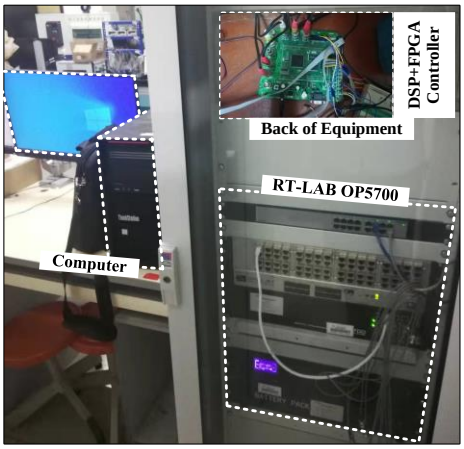

Fig.14. Experimental platform.

Fig.15 shows the experimental results of the studied system when *SCL* is switched from 0 to 45%. As seen from Fig.15, the currents i_{Labc} oscillate first and then return to the stability. Compared with the current, the voltage does not appear an

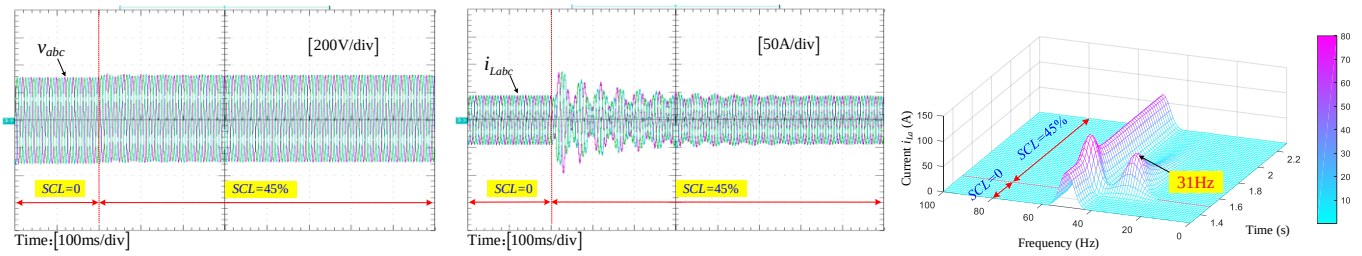

(a) (b) (c)

Fig.15. Experimental results of the studied system when *SCL* is switched from 0 to 45%. (a) PCC voltages. (b) Grid currents. (c) Current spectrums.

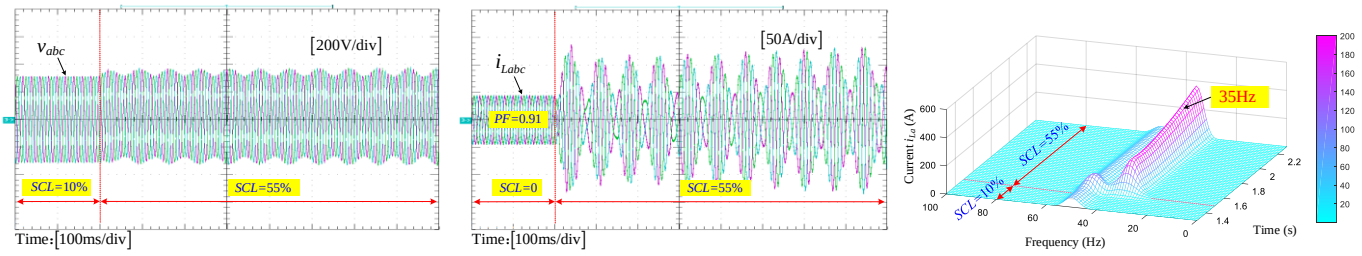

(a) (b) (c)

Fig.16. Experimental results of the studied system when *SCL* is switched from 10% to 55%. (a) PCC voltages. (b) Grid currents. (c) Current spectrums.

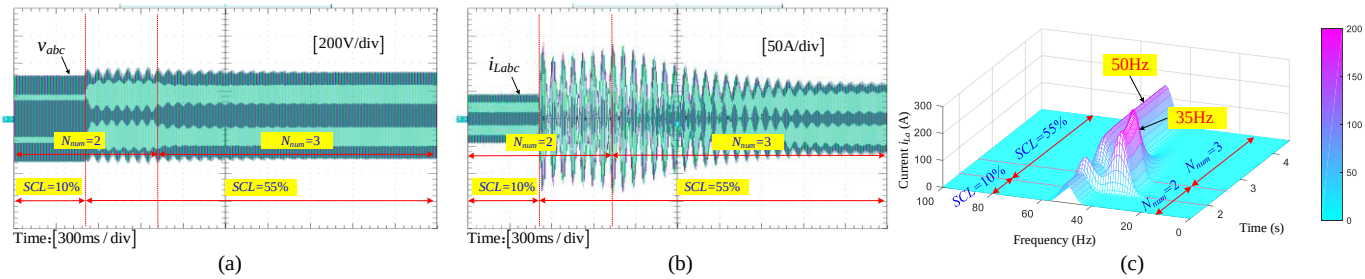

(a) (b) (c)

Fig.17. Experimental results of the studied system when N_{num} is increased from 2 to 3. (a) PCC voltages. (b) Grid currents. (c) Current spectrums.

This article has been accepted for publication in IEEE Transactions on Power Systems. This is the author's version which has not been fully edited and content may change prior to final publication. Citation information: DOI 10.1109/TPWRS.2022.3191061

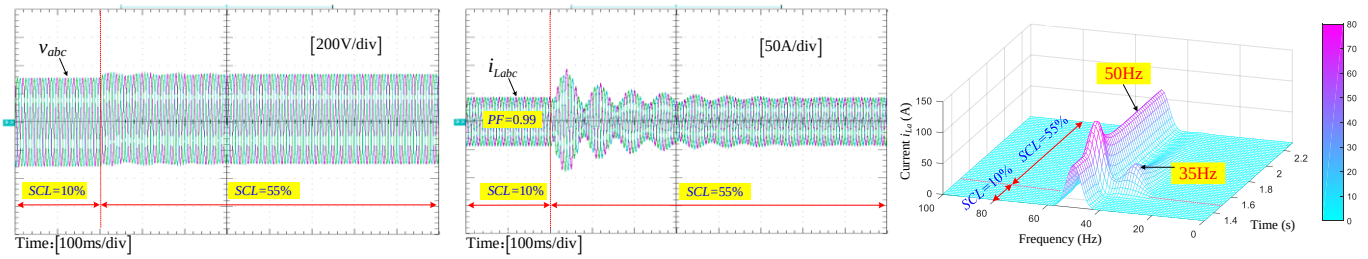

(a) (b) (c)

Fig.18. Experimental results of the studied system with the proposed APF when *SCL* is switched from 10% to 55%. (a) PCC voltages. (b) Grid currents. (c) Current spectrums.

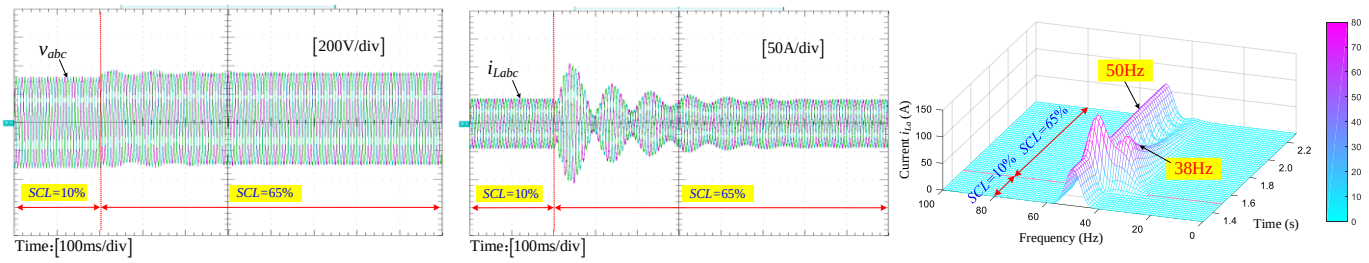

(a) (b) (c)

Fig.19. Experimental results of the studied system with the proposed APF when *SCL* is switched from 10% to 65%. (a) PCC voltages. (b) Grid currents. (c) Current spectrums.

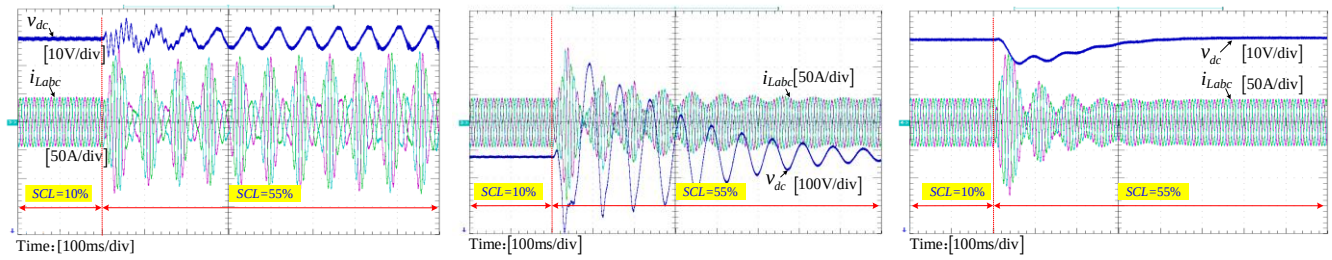

(a) (b) (c)

Fig.20. Experimental results of the studied system with different APF. (a) APF in [30]. (b) Proposed APF with C_{dc}=0.001F. (c) Proposed APF with C_{dc}=0.1F.

obvious oscillation. Form Fig.15(c), the oscillation frequency of current is mainly 31Hz. In addition, Fig.16 shows the experimental results of the studied system when *SCL* is switched from 10% to 55%. As seen from Fig.16, the PCC voltages v_{abc} and the currents i_{Labc} both seriously oscillate. Form Fig.16(c), the oscillation frequency of current is mainly 35Hz, which is higher than that of system with *SCL*=45%. Owing to the impedance interaction between the synchronverter based wind farm and series compensated transformation line, the synchronverter based wind farm is prone to cause SSO. The induced oscillation frequency of system will be higher when the *SCL* is higher. Moreover, from Fig.17, when the number of parallel synchronverters is increased from 2 to 3, the SSO gradually disappear. Based on the analysis above, within a certain tolerance, the experimental results are consistent with the impedance network model based SSO analysis in Section II.

Fig.18 and 19 show the experimental results of the studied system with the proposed APF. As seen from Fig.18, after adding the designed APF, the SSO of synchronverter based wind farm can be effectively suppressed. Simultaneously, the power factor (PF) is corrected from 0.91 to 0.99. Seen from Fig.19, when *SCL* is switched from 10% to 65%, the SSO of synchronverter based wind farm can also be mitigated. In addition, the system oscillation frequency is about 38Hz, which is higher than 35Hz in Fig.18. From Fig.18 and 19, the proposed APF can automatically suppress the SSO and compensate reactive power. The experimental results are consistent with the theoretical analysis, which verifies the feasibility of the proposed strategy.

Fig.20 shows the contrast experimental results of the studied system with different APFs. Seen from Fig.20 (a), the introduced APF in [30] cannot suppress the SSO. Since the control bandwidth of voltage loop is larger than that of the SSO frequency, the dc-side voltage of APF will fluctuate and it cannot suppress SSO. Compared Fig.20(b) and Fig.20(c), the dc-side voltage v_{dc} of the proposed APF slightly fluctuates when the dc-side capacitor is larger. To make the dc-side voltage fluctuates within a certain range, the dc-side capacitor of the proposed APF should be large enough. The experimental results are consistent with the theoretical analysis, which verifies the effectiveness of the proposed SSO suppression method.

V. Conclusion

In this paper, the SSO of the synchronverter based wind farm connected to series compensated transmission line are studied. Some conclusions are listed below.

1) Due to the impedance interaction between the synchron-

verter based wind farm and the series compensated transmission line, the synchronverter based wind farm can cause SSO. With the increase of *SCL*, the stability of the synchronverter based wind farm becomes worse and the induced SSO frequency increases.

2) Owing to the power conservation and the small control bandwidth, the designed first-order inertial controller of the voltage loop can automatically and accurately obtain the active current amplitude. Moreover, when the dc-side capacitance is large enough, the dc-side voltage of the proposed APF fluctuates within the allowable range and then it can efficiently suppress SSO.

3) Since the generalized harmonic current includes the reactive current and the distorted current, the proposed APF has a wide application prospect, such as SSO mitigation, harmonics suppression and reactive compensation.

References

[1] Q.-C. Zhong and G. Weiss, "Synchronverters: Inverters that mimic synchronous generators," *IEEE Trans. Ind. Electron*., vol. 58, no. 4, pp. 1259–1267, Apr. 2011.

[2] M. Ramezani, S. Li, F. Musavi and S. Golestan, "Seamless Transition of Synchronous Inverters Using Synchronizing Virtual Torque and Flux Linkage," *IEEE Trans. Ind. Electron*., vol. 67, no. 1, pp. 319–328, Jan. 2020.

[3] G. Li, F. Ma, Y. Wang, M. Wen, Z. Chen and X. Li, "Design and Operation Analysis of Virtual Synchronous Compensator," *IEEE J. Emerg. Sel. Topics Power Electron*., vol. 8, no. 4, pp. 3835-3845, Dec. 2020.

[4] H. Wu, X. Ruan. D. Yang, X. Chen, W Zhao, Z. Lv and Q.-C. Zhong, "Small-signal modeling and parameters design for virtual synchronous generators," *IEEE Trans. Ind. Electron*., vol. 63, no. 7, pp. 4292-4303, Jul. 2016.

[5] S. Dong, J. Jiang and Y. Chen, "Analysis of Synchronverter Self-synchronization Dynamics to Facilitate Parameter Tuning," *IEEE Trans. Energy. Convers*., vol. 35, no. 1, pp. 11-23, Mar. 2020.

[6] G. Li, F. Ma, A. Luo, Z. He, W. Wu, X. Wei, Z. Zhu, and J. Guo, "Virtual impedance-based virtual synchronous generator control for grid-connected inverter under the weak grid situations," *IET Power Electron*., vol. 11, no. 13, pp. 2125-2132, Nov. 2018.

[7] S. D'Arco and J. Suul, "Virtual synchronous machines–classification of implementations and analysis of equivalence to droop controllers for microgrids," in *IEEE Grenoble Conference*, Grenoble, France, Jun. 2013, pp. 1-7.

[8] W. Wu, Y. Chen, L. Zhou, A. Luo, X. Zhou, Z. He, L. Ying, Z. Xie, J. Liu and M. Zhang, "Sequence Impedance Modeling and Stability Comparative Analysis of Voltage-Controlled VSGs and Current-Controlled VSGs," *IEEE Trans. Ind. Electron*., vol. 66, no. 8, pp. 6460-6472, Aug, 2019.

[9] G. Li, Y. Chen, A. Luo, Z. He, H. Wang, W. Wu and L. Zhou, "Analysis and Mitigation of Sub-synchronous Resonance in Series-Compensated Grid-Connected System Controlled by Virtual Synchronous Generator," *IEEE Trans. Power Electron*., vol.35, no. 10, pp. 11096-11107, Oct. 2020.

[10] J. V. Milanovic and A. Adrees, "Identifying Generators at Risk of SSR in Meshed Compensated AC/DC Power Networks," *IEEE Trans. Power Syst*., vol.28, no.4, pp. 4438-4447, Nov. 2013.

[11] B. Shao, S. Zhao, Y. Yang, B. Gao, L. Wang and F. Blaabjerg, "Nonlinear Sub-synchronous Oscillation Damping Controller for Direct-drive Wind Farms with VSC-HVDC Systems," *IEEE J. Emerg. Sel. Topics Power Electron*., doi: 10.1109/JESTPE.2020.3025081.

[12] D. Yang, X. Wang, F. Liu, K. Xin, Y. Liu and B. Frede, "Symmetrical PLL for SISO Impedance Modeling and Enhanced Stability in Weak Grids," *IEEE Trans. Power Electron*., vol. 35, no. 2, pp. 1473-1483, Feb. 2020.

[13] M. Morshed, and A. Fekih, "A Probabilistic Robust Coordinated Approach to Stabilize Power Oscillations in DFIG-Based Power Systems," *IEEE Trans. Ind. Informat*., vol.34, no.6, pp. 4913-4943, Nov. 2019.

[14] W. Liu, X. Xie, J. Shair, H. Liu and J. He, "Frequency-coupled impedance model-based sub-synchronous interaction analysis for direct-drive wind turbines connected to a weak AC grid," *IET Renew. Power Gener*., vol.13, no.16, pp. 2996-2976, Dec. 2019.

[15] H. Liu, X. Xie, X. Gao, H. Liu and Y. Li, "Stability Analysis of SSR in Multiple Wind Farms Connected to Series-Compensated Systems Using Impedance Network Model," *IEEE Trans. Power Syst*., vol. 33, no. 3, pp. 3118-3128, May. 2018.

[16] B. Badrzadeh, M. Sahni, Y. Zhou, D. Muthumuni and A. Gole, "General Methodology for Analysis of Sub-Synchronous Interaction in Wind Power Plants," *IEEE Trans. Power Syst*., vol. 28, no.2, pp. 1858-1869, May, 2013.

[17] Y. Zhan, X. Xie and Y. Wang, "Impedance Network Model Based Modal Observability and Controllability Analysis for Renewable Integrated Power Systems," *IEEE Trans. Power Del*., vol. 36, no. 4, pp. 2025-2034, Aug. 2021.

[18] I. B. M. Matsuo, F. Salehi, L. Zhao, Y. Zhou and W. Lee, "Optimized Frequency Scanning of Nonlinear Devices Applied to Subsynchronous Resonance Screening," *IEEE Trans. Ind. Appl*., vol. 56, no. 3, pp. 2281-2291, May. 2020.

[19] Y. Zhang, X. Chen and J. Sun, "Sequence Impedance Modeling and Analysis of MMC in Single-Star Configuration," *IEEE Trans. Power Electron*., vol. 35, no. 1, pp. 334-346, Jan. 2020.

[20] G. Li, Y. Chen, A. Luo and X. Liu, "Wideband Harmonic Voltage Feedforward Control Strategy of STATCOM for Mitigating Sub-synchronous Resonance in Wind Farm Connected to Weak Grid and LCC HVDC," *IEEE J. Emerg. Sel. Topics Power Electron*., vol. 9, no. 4, pp. 4546-4557, Aug. 2021.

[21] G. Li, Y. Chen, A. Luo and Y. Wang, "An Inertia Phase Locked Loop for Suppressing Sub-synchronous Resonance of Renewable Energy Generation System under Weak Grid," *IEEE Trans. Power Syst.*, vol. 36, no. 5, pp. 4621-4631, Sep. 2021.

[22] B. Shao, S. Zhao, Y. Yang, B. Gao, L. Wang and F. Blaabjerg, "Nonlinear Sub-synchronous Oscillation Damping Controller for Direct-drive Wind Farms with VSC-HVDC Systems," *IEEE J. Emerg. Sel. Topics Power Electron*., doi: 10.1109/JESTPE.2020.3025081.

[23] T. Joseph, C. E. Ugalde-Loo, S. Balasubramaniam, J. Liang and G. Li, "Experimental Validation of an Active Wideband SSR Damping Scheme for Series-Compensated Networks," *IEEE Trans. Power Del*., vol. 35, no. 1, pp. 58-70, Feb. 2020.

[24] A. Moharana, R. K. Varma and R. Seethapathy, "SSR Alleviation by STATCOM in Induction-Generator-Based Wind Farm Connected to Series Compensated Line," *IEEE Trans. Sustain. Energy*., vol. 5, no. 3, pp. 947–957, Jul. 2014.

[25] G. Li, Y. Chen, A. Luo and H. Wang, "An Enhancing Grid Stiffness Control Strategy of STATCOM/BESS for Damping Sub-synchronous Resonance in Wind Farm Connected to Weak Grid," *IEEE Trans. Ind. Informat*., vol.16, no.9, pp. 5835-5845, Sep. 2020.

[26] L. Wang, X. Xie, Q. Jiang and H. R. Pota, "Mitigation of Multimodal Subsynchronous Resonance Via Controlled Injection of Supersynchronous and Subsynchronous Currents," *IEEE Trans. Power Syst.*, vol. 29, no.3, pp. 1335-1344, May, 2014.

[27] T. Joseph, C. E. Ugalde-Loo, S. Balasubramaniam, J. Liang and G. Li, "Experimental Validation of an Active Wideband SSR Damping Scheme for Series-Compensated Networks," *IEEE Trans. Power Del*., vol. 35, no. 1, pp. 58-70, Feb. 2020.

[28] X.Zhang, X. Xie, X. Li, J. Shair and C. Liu, "Supplementary Damping Control of STATCOM to Mitigate SSCI," *IEEE PES Innovative Smart Grid Technologies Asia*., 2019.

[29] B. Gao and Y. Hu, "Sub-synchronous resonance mitigation by a STATCOM in doubly fed induction generator-based wind farm connected to a series-compensated transmission network," *J. Eng.*, vol. 2019, no. 16, pp. 812-815, Mar. 2019.

[30] S. Hou, Y. Chu and J. Fei, "Intelligent Global Sliding Mode Control Using Recurrent Feature Selection Neural Network for Active Power Filter," *IEEE Trans. Ind. Electron*., vol. 68, no. 8, pp. 7320-7329, Aug. 2021.

[31] Y. Wang, L. Wang and Q. Jiang, "Impact of Synchronous Condenser on Sub/Super-Synchronous Oscillations in Wind Farms," *IEEE Trans. Power Del*., vol. 36, no. 4, pp. 2075-2084, Aug. 2021.

This article has been accepted for publication in IEEE Transactions on Power Systems. This is the author's version which has not been fully edited and content may change prior to final publication. Citation information: DOI 10.1109/TPWRS.2022.3191061

Gaoxiang Li (Member, IEEE) was born in Henan, China, 1990. He received the B.S. degree in electrical engineering and automation from the School of Electrical Engineering and Automation, Henan Polytechnic University, Jiaozuo, China, in 2014. He received the M.S. degree in electrical engineering from the College of Information science and Engineering, Central South University, Changsha, China, in 2017. He received the Ph.D. degree in electrical engineering from Hunan University, Changsha, China, in 2021. He has been an associate Professor in the College of Electrical Engineering, Guangxi University, Nanning.

His research interests include power electronics modeling and control, renewable energy generation, energy storage.

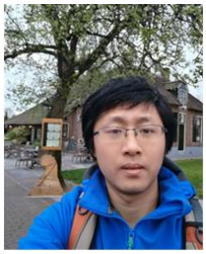

Fujun Ma (M'15) was born in Hunan, China, 1985. He received the B.S. degree in Automation and Ph.D. degree in Electrical Engineering from Hunan University, Changsha, in 2008 and 2015, respectively. Since 2016, he has been an Associate Professor with the College of Electrical and Information Engineering, Hunan University.

His research interests include power quality managing technique of electrified railway, electric power saving, reactive power compensation, and active power filters.

Chuanping Wu was born in Hunan, China, in March 1984. He received the M.S. and Ph.D. degrees from the College of Electrical and Information Engineering, Hunan University, Changsha, China, in 2007 and 2012, respectively. In 2012, he joined State Key Laboratory of Disaster Prevention and Reduction for Power Grid Transmission and Distribution Equipment (Disaster Prevention and Reduction Center of State Grid Hunan Electric Power Company).

His research interests include power quality control technique for electric system, DC de-icing technique for transmission lines, and disaster prevention technique for power grid.

Mingshen Li (Graduate Student Member, IEEE) received the B.S. degree in electrical engineering from Chongqing University, Chongqing, China, in 2013, and the M.S. degree in electrical engineering from the College of Electrical and Information Engineering, Hunan University, Changsha, in 2016. He is currently working toward the Ph.D. degree in power electronics systems with the Department of Energy Technology, Aalborg University, Aalborg, Denmark.

His current research interests include primary control of converters, microgrid cluster systems, and distributed generation systems.

Josep M. Guerrero (S'01-M'04-SM'08-FM'15) received the B.S. degree in telecommunications engineering, the M.S. degree in electronics engineering, and the Ph.D. degree in power electronics from the Technical University of Catalonia, Barcelona, in 1997, 2000 and 2003, respectively. Since 2011, he has been a Full Professor with the Department of Energy Technology, Aalborg University, Denmark. From 2015 he is a distinguished guest Professor in Hunan University. His research interests mainly include power electronics, distributed energy-storage, and microgrids. Prof. Guerrero is an Associate Editor for the IEEE TRANSACTIONS ON POWER ELECTRONICS, the IEEE TRANSACTIONS ON INDUSTRIAL ELECTRONICS, and the IEEE Industrial Electronics Magazine, and an Editor for the IEEE TRANSACTIONS on SMART GRID and IEEE TRANSACTIONS on ENERGY CONVERSION. In 2014, 2015, and 2016 he was awarded by Thomson Reuters as Highly Cited Researcher, and in 2015 he was elevated as IEEE Fellow for his contributions on distributed power systems and microgrids.

Man-Chung Wong (Senior Member, IEEE) received the B. Sc. and M. Sc. degrees in Electrical and Electronics Engineering from the University of Macau (UM), Macao, China in 1993 and 1997 respectively and Ph.D. degree in Electrical Engineering from Tsinghua University, Beijing, China in 2003.

He is currently a Professor with the Department of Electrical and Computer Engineering, UM, and also is affiliated with the State Key Laboratory of Internet of Thing Smart City and State Key Laboratory of Analog and Mixed-Signal VLSI, UM. He was a Visiting Fellow with Cambridge University.